Materials Today Physics 54 (2025) 101712

Contents lists available at ScienceDirect

Materials Today Physics

journal homepage: www.journals.elsevier.com/materials-today-physics

Enhanced thermopower by double-site substitution of Ti in $Fe_2(VAl)_{1-x}Ti_{2x}$

M. Parzer [a,*], A. Kositz [a], J. Süß [a], F. Garmroudi [a,b], T. Mori [c,d], E. Bauer [a]

[a] Institute of Solid State Physics, Technische Universität Wien, 1040 Vienna, Austria
[b] Materials Physics and Applications – Quantum, Los Alamos National Laboratory, Los Alamos, NM 87545, USA
[c] International Center for Materials Nanoarchitectonics (WPI-MANA), National Institute for Materials Science (NIMS), Tsukuba, Japan
[d] Graduate School of Pure and Applied Science, University of Tsukuba, Tsukuba, Japan

ARTICLE INFO

Keywords:
Thermoelectricity
Thermoelectric materials
Transport properties
Transport modeling
Electronic structure

ABSTRACT

Thermoelectric (TE) materials, which directly convert heat into electricity, hold promise for sustainable energy applications. For widespread adoption of this technology, the development of efficient, cost-effective, and non-toxic TE materials is crucial. Here, we attempt to improve the thermoelectric properties of Fe_2VAl-based full-Heusler compounds through the targeted substitution of (VAl) by Ti_2 in $Fe_2(VAl)_{1-x}Ti_{2x}$. Our study reveals a miscibility gap between $0.4 < x < 0.9$, yet significant enhancement of the thermoelectric performance for both *p*- and *n*-type compounds was achieved for smaller substitutions. While Fe_2VAl and Fe_2Ti_2 are semimetals, a band gap opening occurs in the solid solution series, yielding a substantial enhancement of the Seebeck coefficient up to 130 μV/K in *p*-type materials. By additional optimization via isovalent V/Ta heavy-element substitution, we further optimize the TE performance, achieving one of the best zT values in *p*- and *n*-type full-Heusler compounds and revealing the (VAl)/Ti_2 substitution as a promising pathway for improving the TE efficiency of full-Heusler compounds.

1. Introduction

Thermoelectricity is a diverse research field, very close to both application but also fundamental materials science. Various thermoelectric materials are being explored for power generation applications, such as GeTe [1], Bi_2Te_3 [2], PbTe [3,4], and half-Heusler compounds [5]. The efficiency of a thermoelectric generator is guided by the figure of merit $zT = (\sigma S^2/\kappa)T$, where S denotes the Seebeck coefficient, σ the electrical and κ the thermal conductivity, respectively. The zT is an inherently material-dependent property which must be increased in order to enhance the efficiency and therefore the feasibility of thermoelectric generators. Aside of the zT, other material's properties, like element price, chemical and mechanical stability as well as workability are important parameters, impacting the applicability of thermoelectric materials. In the light of these requirements, Fe_2VAl-based full-Heusler materials emerged as potential candidates for thermoelectric applications and have been investigated extensively in recent years [6–13]. These materials feature cheap and abundant constituent elements, high stability, as well as an extremely high electronic power factor ($PF = \sigma S^2$), up to 10.3 W/mK^2 [14], which is prerequisite for achieving high zT values. The downside of Fe_2VAl-based materials is the high lattice thermal conductivity, but also the relatively low Seebeck coefficient S. As detailed in Ref. [15] this leads to lower maximum zT values in these compounds, especially for *p*-type Fe_2VAl-based materials.

To overcome this challenge, here, the gradual substitution of (VAl) with Ti_2 in Fe_2VAl is systematically investigated up to the phase boundary of FeTi. Notably, both materials are stable semimetals with a deep pseudogap at the Fermi level E_F, crystallizing in nearly identical B2-type cubic crystal structure. Through rational chemical considerations and an understanding of the electronic structure of the two end compounds, it is anticipated that the double-site substitution could significantly increase the thermoelectric (TE) performance of the compounds by opening a band gap in the intermediate compounds. In this work, the whole compositional phase space of $Fe_2(VAl)_{1-x}Ti_{2x}$ from $x = 0$–1 was screened by synthesizing slightly *n*- and *p*-doped samples, which were characterized regarding their homogeneity and their TE performance.

2. Concept

The study was motivated by the apparent similarity between Fe_2VAl and FeTi, which crystallize into the highly ordered $L2_1$ (Heusler) and the partially disordered B2 structure (a higher symmetry version of the $L2_1$ structure), respectively. Its chemical stability is confirmed

* Corresponding author.
E-mail address: michael.parzer@tuwien.ac.at (M. Parzer).

https://doi.org/10.1016/j.mtphys.2025.101712
Received 14 January 2025; Received in revised form 26 March 2025; Accepted 29 March 2025
Available online 11 April 2025
2542-5293/© 2025 The Authors. Published by Elsevier Ltd. This is an open access article under the CC BY license (http://creativecommons.org/licenses/by/4.0/).

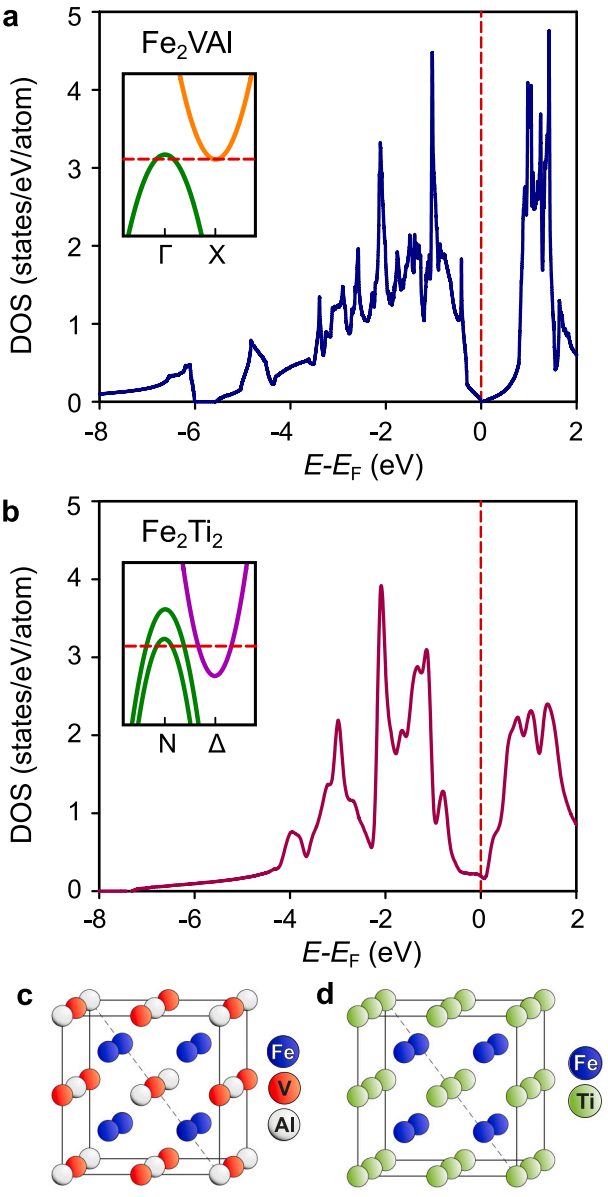

Fig. 1. Concept of (VAl)/Ti_2 substitution Panels (a) and (b) depict the electronic densities of states (DOS) of Fe_2VAl and FeTi, respectively, taken from *The Materials project* [16]. Evidently, both compounds exhibit a semimetallic DOS with a profound pseudogap at the Fermi level E_F. The inset depicts a sketch of the electronic band structure close to the Fermi level. Both compounds feature a slight overlap of valence and conduction band, however, at different points in the Brillouin zone and from different orbitals. Panels (c) and (d) depict the crystal structures of Fe_2VAl and Fe_2Ti_2 ordering in the $L2_1$ and B2 structure, respectively.

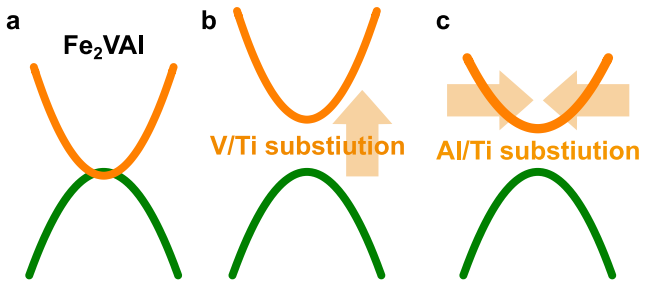

Fig. 2. Effects of V/Ti and V/Al substitutions Panel (a) depicts a sketch of the effective band structure of Fe_2VAl close to the Fermi level E_F, exhibiting a small band overlap. Panels (b) and (c) illustrate the effect of V/Ti and V/Al substitution, respectively. For V/Ti, the hybridization of 3d states from Ti and V leads to a shift of the conduction band to higher energies. For V/Al substitution, the distortion of the V–V bonding leads to a flatter conduction band, effectively opening the band gap.

experimentally by Fe–Ti phase diagrams [17], readily available for the binary compound, but also from old reports on the mechanical properties of FeTi [18,19].

Doubling the unit cell and rewriting the chemical formula as Fe_2Ti_2, the similarity of the compound to the Heusler stoichiometry X_2YZ becomes apparent, with the Z atoms (typically a main group element) substituted by the Y element leading to an X_2Y_2 stoichiometry.

Remarkably, FeTi exhibits a valence electron count of 6 e^-/atom, similar to Fe_2VAl, as Ti possesses 4 valence electrons, constituting the middle point between V (5 e^-) and Al (3 e^-). Following the Slater–Pauling (S–P) rule for Heusler compounds [20,21], which states that materials with six valence electrons per atom are nonmagnetic semiconductors, this hints at the possibility that FeTi exhibits a semiconducting or semimetallic ground state. Indeed, density-functional theory calculations predict Fe_2VAl and FeTi as semimetals. The electronic density of states (DOS) of Fe_2VAl and FeTi are depicted in Fig. 1a,b as extracted from *The Materials project* [16]. Clearly, a notable dent in the DOS of Fe_2Ti_2 is discernible around the Fermi level E_F, similar to Fe_2VAl. While the number of states at the Fermi level is higher than for the latter, the pseudo-gap is still present. Moreover, in accordance with the S–P rule regarding magnetic ordering, FeTi is not ferromagnetic.

Obviously, FeTi and Fe_2VAl are similar compounds with similar electronic structure and magnetic properties. As highlighted in Fig. 1c,d, depicting the two crystal structures, Fe_2VAl can directly be translated to FeTi by simply substituting (VAl) with two Ti atoms. Moreover, the simultaneous substitution of (VAl) with 2 Ti atoms inherently keeps the valence electron concentration constant, implying a lack of electron or hole doping and a fixation of the Fermi level along the transition from Fe_2VAl to Fe_2Ti_2.

Therefore, the changes in the electronic band structure and transport properties are expected to be of intrinsic nature by changing the hybridization between atoms and the available electronic states. The constant VEC makes it that the impact of the (VAl)/Ti_2 substitution on the electronic band structure can directly be analyzed from the substitution studies. We expect two competing effects occurring simultaneously, which are illustrated in Fig. 2b,c for V/Ti and Al/Ti substitution:

As highlighted in the inset of Fig. 1a, the band gap in Fe_2VAl is determined by the energy gap between the Fe-dominated valence band located at the Γ point and the V-dominated conduction band situated at X. As Ti has its 3d states at significantly higher energies, the replacement of V atoms with Ti leads to an overall shift of the conduction band towards higher energies, as the V and Ti states hybridize, effectively opening a band gap. This effect has already been showcased in previous studies of Ti substitution in Fe_2VAl-based materials [6,11].

On the other hand, it is the transition-metal hybridization with the Al atoms, together with the lack of Al d–d hybridization that leads to the deep pseudogap in Fe_2VAl [22]. While Al atoms feature negligible amounts of states around E_F, it is the bonding with Fe and V that induces the extensive pseudogap in the compound. This has recently been demonstrated for off-stoichiometric Fe_2VAl [23].

Hence, the impact of substituting (VAl) by Ti_2 is twofold: The V-dominated band at the X point hybridizes with the substituent Ti atoms and is therefore shifted towards higher energies. At the same time, the substitution of the main group element Al with Ti leads to stronger $d-d$ hybridization between the transition metal atoms as the average interatomic distance is reduced, broadening the bandwidth and thereby closing the pseudogap.

Notably, both effects lead to a significant pseudogap in the end compounds Fe_2VAl and Fe_2Ti_2. The interplay of band structure modifications can lead to a band gap opening for intermediate compounds, if

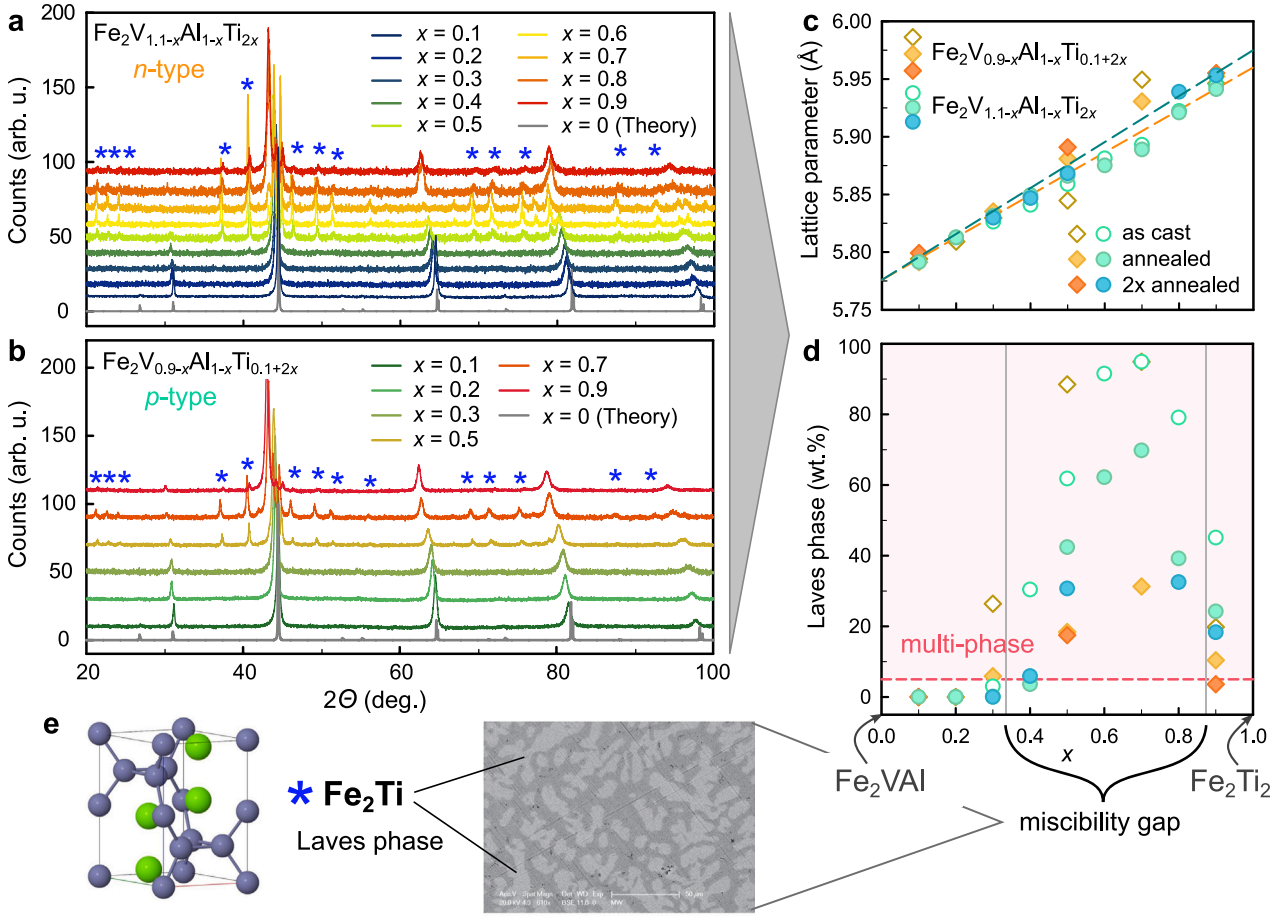

Fig. 3. XRD results of $Fe_2V_{0.9-x}Al_{1-x}Ti_{0.1+2x}$ Panels (a) and (b) display the measured X-ray diffraction (XRD) patterns the compounds along the $Fe_2V_{0.9-x}Al_{1-x}Ti_{0.1+2x}$ and $Fe_2V_{1.1-x}Al_{0.9-x}Ti_{2x}$ stoichiometries, ranging from $x = 0.1$ to 0.9. The patterns depicted are the ones after the final annealing step, as detailed in the text. The gray line depicts the theoretical symmetry peaks of the $L2_1$ full-Heusler structure, while the blue asterisks mark the symmetry peak of the hexagonal Fe_2Ti Laves phase. Evidently, intermediate samples ($0.4 < x < 0.9$) exhibit a substantial amount of Laves second phase up to $Fe_2Ti_{1.9}Al_{0.1}$ ($x = 0.9$) for the *p*-type compounds, which is close to being single-phase. Panel (c) shows the lattice parameters of the different compounds, determined via Rietveld refinement after each annealing step. Evidently, the annealing leads to the convergence of the lattice parameters towards the linear scaling in accordance to Vegard's law. Panel (d) depicts the amount of Laves phase present in the samples after each annealing step in percent, determined from Rietveld refinement. A significant miscibility gap is evident between $x = 0.4$ and $x = 0.9$, where the formation of the Laves phase introduces a considerable amount of a second phase in the samples from both series. Panel (e) shows the crystal structure of the Fe_2Ti second phase, together with a back-scattered electron image of the *p*-type sample with $x = 0.5$. The phase separation is distinctly observable, with the Laves phases appearing as brighter regions that form dendritic-shaped areas.

the two partial effects combine beneficially for $0 < x < 1$. This is particularly compelling, as the highest figure of merit zT for *p*-type Heusler compounds was found in the compound $Fe_2V_{0.69}Ti_{0.34}Ta_{0.05}Al_{0.92}$, which includes a substantial amount of Ti [6]. Notably, the successful doping study on $Fe_2V_{1.08-y}Ti_yAl_{0.92}$, shows similarities to the idea of (VAl)/Ti_2 substitution for higher y. Therefore, partially substituting (VAl) with Ti atoms presents a promising strategy to enhance the thermoelectric performance, particularly in increasing $S(T)$ in full-Heusler compounds.

To systematically investigate the effects of (VAl)/Ti_2 substitution, we synthesized and characterized both *p*- and *n*-doped samples along this stoichiometry. This approach ensures that the samples are already near optimal thermoelectric performance, allowing us to analyze the modifications in both the valence and conduction bands.

For *p*-type compounds, samples along the stoichiometry $Fe_2V_{0.9-x}Al_{1-x}Ti_{0.1+2x}$ were prepared, including $Fe_2V_{0.9}Ti_{0.1}Al$ for $x = 0$. This compound has been investigated previously and features a high power factor, but relatively low Seebeck coefficient S [24]. To evaluate the effect of (VAl)/Ti_2 substitutions in *n*-type compounds, we synthesized samples along the stoichiometry $Fe_2V_{1.1-x}Al_{0.9-x}Ti_{2x}$, and compared them to the baseline compound $Fe_2V_{1.1}Al_{0.9}$ at $x = 0$. The V-Al off-stoichiometry is well investigated and samples along $Fe_2V_{1+x}Al_{1-x}$ feature high thermoelectric power factors alongside decently high Seebeck coefficients [9,12,25,26].

3. Experimental results

In the following section, we will examine the structure and phase stability of these compounds, as well as analyze their thermoelectric properties, to assess their potential as efficient thermoelectric materials. All samples were weighed using a high-precision scale and subsequently melted in a high-frequency induction furnace, with weight losses remaining below 0.1% after complete melting. This process has also been validated in previous studies [8,14,27].

3.1. Structural characterization

To investigate the stability and physical properties of compounds along the $Fe_2V_{0.9-x}Al_{1-x}Ti_{0.1+2x}$ and $Fe_2V_{1.1-x}Al_{0.9-x}Ti_{2x}$ stoichiometries, multiple samples with $x = 0.1$, 0.2, 0.3, 0.5, 0.7 and 0.9 were synthesized via induction-melting and annealed in multiple steps. For the *n*-type series, also samples with $x = 0.4$, 0.6 and 0.8 were synthesized to better resolve the phase space of the substitution. X-ray diffraction (XRD) analyses were conducted for as-cast samples as well as after each annealing step. The annealing program was structured the following way: All samples were annealed for 7 days at 800 °C; for compounds showing a significant amount of secondary phases, an additional annealing step was performed for 7 days at 850 °C to

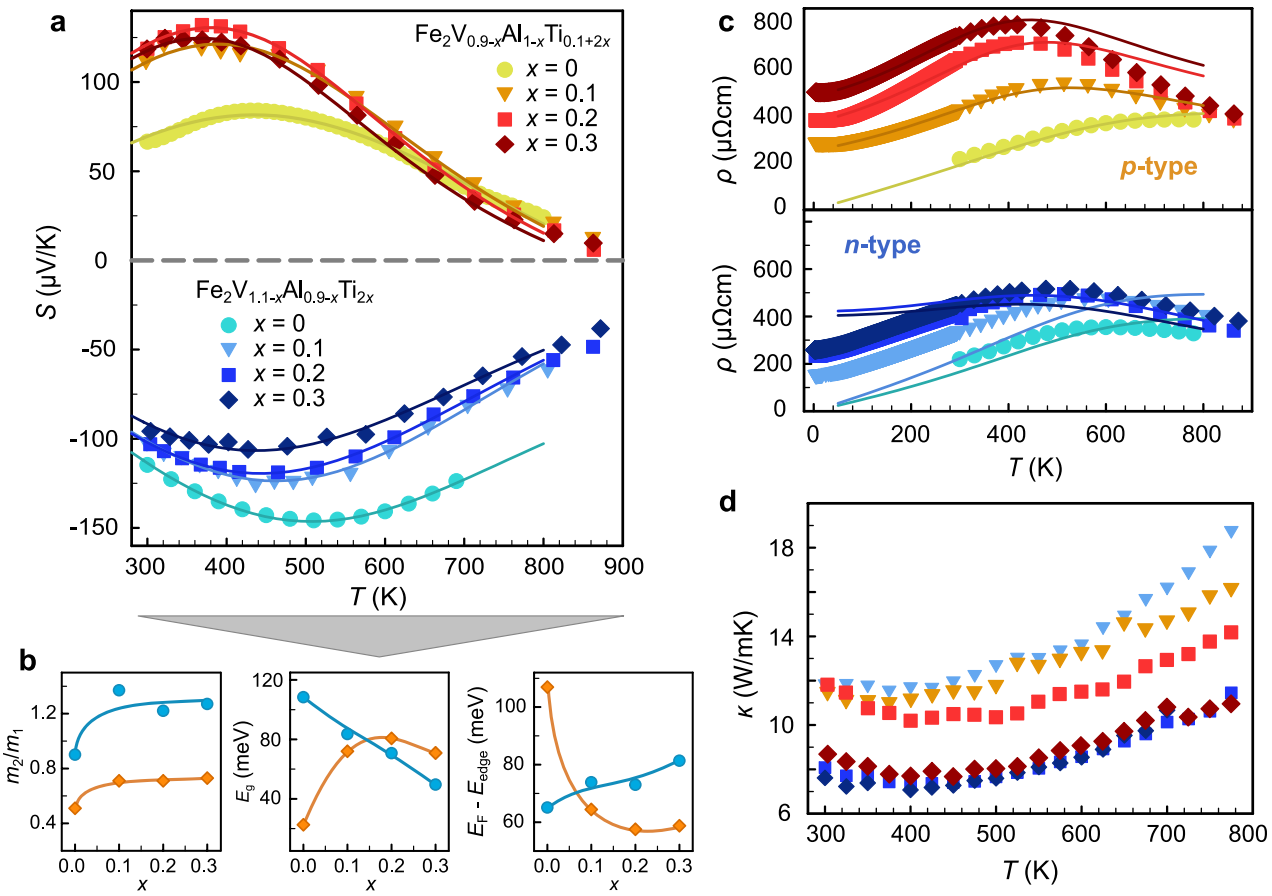

Fig. 4. Thermoelectric properties of $Fe_2V_{0.9-x}Al_{1-x}Ti_{0.1+2x}$. Panel (a) shows the temperature-dependent Seebeck coefficient of *p*- and *n*-type samples up to $x = 0.3$. The solid lines depict the fit results, employing a two-parabolic band model to describe $S(T)$. The graphs in panel (b) delineate the fitting results regarding the mass ratio (m_2/m_1), the band gap (E_g) and the Fermi level (E_F), as detailed in the text. Panels (c) and (d) show the temperature-dependent electrical resistivity $\rho(T)$ and thermal conductivity $\kappa(T)$, respectively. Evidently, the compounds with $x = 0.1$–0.3 not only exhibit similar transport properties, but can also be described with a similar set of fitting parameters. For both sample series, $\rho(T)$ increases continuously with increasing x up to $x = 0.3$.

ensure higher thermal energy for diffusion processes. The measured XRD patterns after the final annealing steps are depicted in Fig. 3a,b, together with the theoretical symmetry peaks for the full-Heusler $L2_1$ structure in gray.

As evidenced by the XRD patterns, both *p*- and *n*-type samples are mostly single-phase up to $x = 0.4$, beyond which slight impurity peaks become visible. Further decreasing the (VAl)/Ti_2 ratio leads to significant impurity peaks, corresponding to the hexagonal C14 Laves structure formed by Fe_2Ti, which is depicted in Fig. 3e. The respective symmetry peaks are marked by the blue asterisks. Similar to the case of Fe_2TiSi [28], the low formation energy of the Fe_2Ti Laves phase inhibits the phase-purity of the intermediate compounds in bulk samples [29]. Scanning electron microscopy (SEM) images confirm the appearance of the secondary phase, with substantial amounts present already for $x = 0.5$ as showcased in Fig. 3f.

The quantitative analysis of the XRD results is presented in Fig. 3c,d. In these figures, the lattice parameters of the compounds, as extracted via Rietveld refinement after the different annealing steps are shown. Moreover, the portion of the secondary phase was determined by evaluating the relative intensities of the peaks corresponding to each phase, taking into account the XRD scattering cross-sections of the constituents. This analysis is summarized in panel d. Not for all samples two annealing steps were necessary; some were single-phase following synthesis or the initial annealing, while others remained too far from single-phase to justify investigation via additional annealing.

For both sample series, the extracted lattice parameters follow linear scaling fairly well, as predicted by Vegard's law [30]. Clearly, with additional annealing, the lattice parameter of the impure samples is approaching linear scaling behavior as more of the Fe_2Ti phase is dissolved into the Heusler main matrix. For the compounds between $x = 0.5$ to 0.9, however, additional annealing did not affect the phase distribution significantly. Hence, the analysis of the phase composition reveals a profound miscibility gap in the domain of the (VAl)/Ti_2 substitution. Notably, the *p*-type $Fe_2Ti_{1.9}Al_{0.1}$ sample ($x = 0.9$) exhibits very small amounts of a second phase, which further decreased after a second annealing step. This suggests that extended annealing might allow for the synthesis of a phase-pure sample of this compound.

3.2. Thermoelectric properties

The thermoelectric properties of the alloys were systematically measured to reveal changes in their electronic structure and determine their thermoelectric figure of merit, zT. Measurements were performed both before and after annealing to evaluate the impact of phase composition on these properties. As the formation of the Laves phase predominantly led to a deterioration of the Seebeck coefficient and zT, only the results obtained after the final annealing steps are presented here. Fig. 4 depicts the temperature-dependent thermoelectric transport properties of the phase-pure samples, ranging from $x = 0$ to $x = 0.3$ for both the *p*- and *n*-type sample series. In Fig. 4a, we show the temperature-dependent Seebeck coefficient $S(T)$ of the respective samples. For the *p*-type materials, shown in yellow to red, $S(T)$ is enhanced significantly with (VAl)/Ti_2 substitution compared to the baseline compound, $Fe_2V_{0.9}Ti_{0.1}Al$, which exhibits a maximum Seebeck coefficient of 80 μV/K. The samples with $x = 0.1$–0.3 display similar $S(T)$ behavior, reaching peak values of approximately 120–130 μV/K

around $T = 350$ to 400 K. In contrast, the (VAl)/Ti_2 substitution leads to a reduction in the absolute $S(T)$ values for the n-type samples based on $Fe_2V_{1.1}Al_{0.9}$. In both cases the maximum of $S(T)$ is shifted towards lower temperatures.

For both series of compounds, samples with higher Ti concentration ($x > 0.4$) are multi-phase and therefore exhibit lower $S(T)$ values alongside a noticeable shift of the peak towards higher temperatures (see Fig. S1 of the Supplemental Material [31] for TE properties of p-type compounds with $x > 0.4$), due to the formation of the metallic Fe_2Ti Laves impurity phase, also altering the composition of the Heusler main matrix.

To analyze the modifications of the transport properties of the phase-pure compounds, the Seebeck coefficient $S(T)$ of all samples was analyzed utilizing a two parabolic band model, as implemented in the software *SeeBand* [32]. In the framework of the parabolic band model, the temperature-dependent Seebeck coefficient of a single band is given by [33]

$$S(T) = \frac{k_B}{e}\left[\eta - \frac{2F_1(\eta)}{F_0(\eta)}\right], \quad (1)$$

with k_B being the Boltzmann constant, e the electronic charge, η the reduced chemical potential and F_i the Fermi integral of ith order. The contribution of two parabolic bands can then be added up using the following equation

$$S_{tot} = \frac{\sigma_1 S_1 + \sigma_2 S_2}{\sigma_1 + \sigma_2}, \quad (2)$$

with S_i and σ_i being the Seebeck coefficient and conductivity of the respective bands, and

$$\sigma_i = \frac{e^2 n \tau_i}{m_i}, \quad (3)$$

with n being the charge carrier concentration, τ_i the scattering time and m_i the band effective mass.

The fit curves are displayed as solid lines in Fig. 4a and yield excellent agreement with the experimental data. As detailed in Ref. [32], the following parameters can be extracted from this procedure: the Fermi level E_F, the band gap E_g and the mass ratio of the two parabolic bands $\epsilon_m = m_2/m_1$. The extracted parameters from the successful fits of $S(T)$ are presented in Fig. 4b for the p- and n-type samples as orange and blue circles as a function of x, respectively.

Both types of compounds display a clear increase of the mass ratio of conduction and valence band, m_{CB}/m_{VB}, caused by the (VAl)/Ti_2 substitution, as shown in Fig. 4b, respectively. Interestingly, the evolution of the band gap with increasing x behaves opposite. While for the p-type samples, the band gap increases significantly for $x = 0.1$ and saturates at higher x, it decreases linearly for the n-type samples. This behavior, displayed in the second panel of Fig. 4b is unexpected, but could be explained by the effects of the V/Ti substitution on the V-dominated conduction band. The increase in m_2 could obscure the band gap opening for the n-type samples, as the weighting of the conduction band is reduced.

Similar behavior is also found for the position of the Fermi level normalized to the corresponding band edge (E_{VB} and E_{CB}), as depicted in the last panel of Fig. 4b. For the n-type samples, the Fermi level, normalized to the respective band edge, is progressively shifted further into the conduction band, while for the p-type samples it jumps closer to the band edge for $x = 0.1$ and remains roughly constant for higher x.

The temperature-dependent resistivity curves $\rho(T)$, shown in Fig. 4c, reveal that for both materials, overall $\rho(T)$ increases with x. Simultaneously, the maximum of $\rho(T)$ is shifted towards lower temperatures. Assuming alloy-disorder scattering, the temperature-dependent resistivity of a single parabolic band can be calculated [33]

$$\rho(T) = \sigma^{-1} = \left[\frac{2\sqrt{2}e^2 k_B T}{\pi^2 \hbar^3}\left(\frac{\tau}{m}\right) F_0(\eta)\right]^{-1}. \quad (4)$$

The total resistivity follows then from the inverse of the sum of the individual conductivity contributions, given by: $\rho_{tot} = \sigma_{tot}^{-1} = (\sigma_1 + \sigma_2)^{-1}$.

Notably, the three fit parameters E_F, E_g and ϵ_m are directly derived from the refinement of $S(T)$, leaving only the scattering times τ_i of the respective bands as fitting parameters. To prevent overfitting, the temperature-dependent resistivity, we further constrained the fit of $\rho(T)$ by setting $\tau_1 = \tau_2$, thereby fixing the scattering times of the bands to be equal. Therefore, the resulting temperature dependence of $\rho(T)$ is solely governed by the fit parameters obtained from the Seebeck coefficient refinement. The remaining parameter τ_{tot} serves as a multiplicative factor, representing the scattering strength, determining the absolute value of $\rho(T)$. Nevertheless, the calculated curves at elevated temperatures align well with the experimental data, particularly for the p-type materials. For the latter, the resistivity continuously increases with increasing x. This trend can be attributed to shorter scattering times, τ, derived from the one-parameter fit of $\rho(T)$. Notably, a similar but less pronounced trend is observable in the n-type samples. For both cases, the shorter τ is likely due to increased disorder from the (VAl)/Ti_2 substitution.

Fig. 4d displays the temperature-dependent thermal conductivity, $\kappa(T)$ for the respective alloys. Evidently, $\kappa(T)$ is decreased consistently with increasing x for both n- and p-type samples. The extracted electronic thermal conductivities and the delineated lattice thermal conductivities are presented in Figs. S2 and S3 of the Supplemental Material. The lattice thermal conductivity is decreased with increasing x. This can be attributed alloy-disorder scattering of the phonons caused by the substitution in accordance with Klemens' model [35,36]. Besides, the substitution of lightweight Al by heavier Ti atoms is expected to decrease the sound velocity and thus, intrinsically, the lattice thermal conductivity. Additionally, the decrease of the electrical conductivity σ brings along the decrease of the electronic thermal conductivity, $\kappa_e = L\sigma T$, where L is the Lorenz number. Consequently, for both sample series the (VAl)/Ti_2 substitution leads to a significant reduction of the overall thermal conductivity $\kappa(T)$, expected to increase the figure of merit zT.

Inspection of the temperature-dependent $zT(T)$ in Fig. 5a reveals that for both series, the compound with the lowest (VAl)/Ti_2 substitution ($x = 0.1$) consistently exhibits the highest figure of merit zT. Notably, zT values for both n- and p-type series surpass those of the origin compounds, with significant improvements over previously reported values in Refs. [24–26].

The double-site substitution of (VAl)/Ti_2 also yields relatively high zT values compared to other Fe_2VAl-based materials. Even without further optimization of carrier concentration or substitutions aimed at reducing lattice thermal conductivity (κ_{lat}), the samples achieve $zT_{max} = 0.125$ for p-type and $zT_{max} = 0.18$ for n-type compounds, respectively.

As discussed in Ref. [6], the disparity between n- and p-type zT values is a persistent issue in Fe_2VAl-based compounds. While the highest zT values for n-type materials reach up to 0.3 [34,37], and even $zT = 0.37$ with advanced nanostructuring methods such as high-pressure torsion [10], p-type samples generally exhibit lower figures of merit between $zT = 0.12 - 0.18$ [6,8]. Thus, the substantial enhancement in $S(T)$ observed for the p-type samples here makes them promising candidates for future optimization aimed at improving the thermoelectric performance of full-Heusler compounds.

4. Optimization via heavy-element doping

Consequently, optimization studies regarding the reduction of κ_{lat} were performed to explore the potential of the thermoelectric performance employing the (VAl)/Ti_2 substitution. Phonon engineering presents a promising approach to enhance thermoelectric efficiency by minimizing κ_{lat} without adversely affecting the electronic transport properties, particularly the electronic power factor PF. In Fe_2VAl-based materials, heavy-element doping has proven to be an effective method for significantly reducing κ_{lat} [6,27,37,38]. This reduction has largely been attributed to a decrease of the Debye temperature,

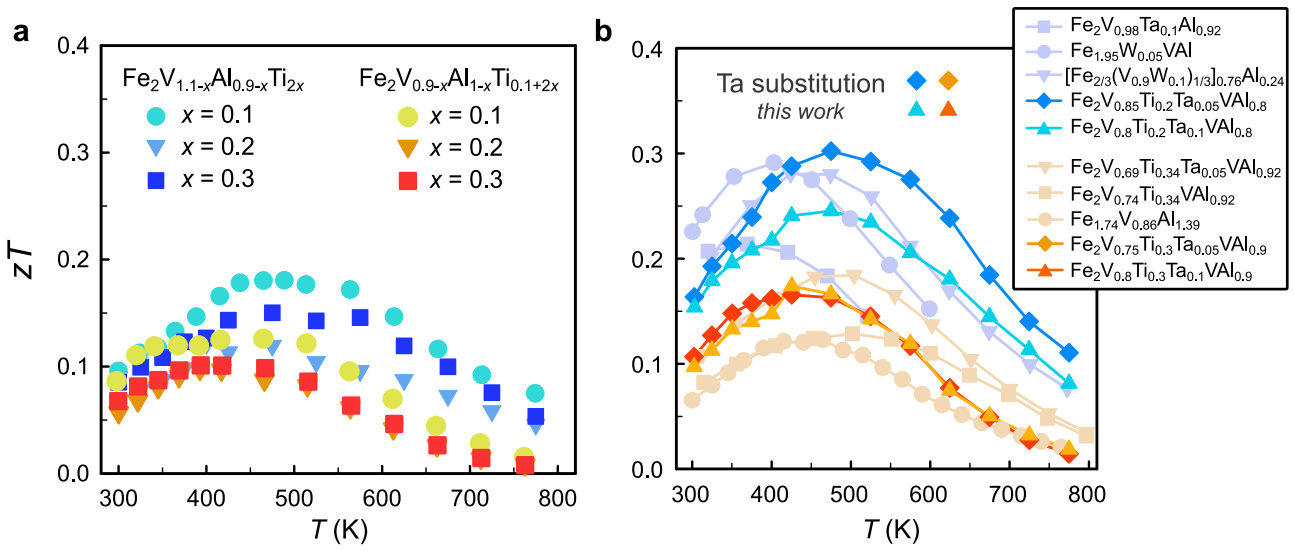

Fig. 5. Thermoelectric figure of merit zT of the two-fold substituted samples Panel (a) displays the temperature-dependent figure of merit zT of the p- and n-type samples along the (VAl)/Ti_2 substitution. In panel (b), we show the enhanced zT of the Ta substituted samples compared with the record-values from literature for substituted Fe_2VAl samples. Evidently, the samples synthesized within this studies constitute some of the best performing thermoelectric full-Heusler materials. The measurement results are compared to literature data extracted from Refs. [6,8,10,27,34].

increased lattice anharmonicity [27] and the emergence of additional phonon modes, particularly in cases of Ta substitution [39].

To further optimize the most promising samples from this study, selective heavy-element doping was employed to enhance the thermoelectric figure of merit (zT). To minimize any adverse effects on electronic transport, isovalent V/Ta substitution was employed, with substitution levels of 5% and 10%. This approach is expected to maintain the position of the Fermi level, ensuring stable electronic properties while decreasing the lattice thermal conductivity κ_{lat}. The results of zT as a function of temperature are presented in Fig. 5b, compared against the highest zT values reported in literature for substituted Fe_2VAl-based compounds. The temperature dependence of individual thermoelectric properties of Ta substituted samples can be seen in Fig. S6 of the Supplemental Material [31].

Overall, the samples preserved similar electronic transport properties to the original compounds, while achieving a substantial reduction of the thermal conductivity. As highlighted in Fig S4 of the Supplemental Material, the lattice thermal conductivity κ_{lat} is almost halved by the small amount of V/Ta substitution. These changes lead to an overall increased figure of merit, with zT values reaching 0.18 and 0.3 for the p- and n-type samples, respectively, peaking around 480 K. Notably, these values are among the highest values reported for Fe_2VAl-based materials [6,37], excluding those obtained through specialized techniques like high-pressure torsion [10]. The strong decrease in thermal conductivity can also be traced back to slight composition variations present in the samples, with very small impurity phases of Fe_2Ta forming, as highlighted in Figs. S7 and S8 of the Supplemental Material [31].

5. Conclusion

We have thoroughly investigated the substitution of (VAl) by Ti_2, progressing from the full-Heusler compound Fe_2VAl to the Heusler-like material Fe_2Ti_2. Despite the semimetallic nature of both compounds, obvious from the densities of states, the prospect of a band gap opening was explored, motivated by rational arguments regarding the electronic structure and chemical bonding. Through careful analysis of phase stability in both p- and n-type samples, subjected to various annealing steps, a pronounced miscibility gap was identified in the range $0.4 < x < 0.9$ for both p-type $Fe_2V_{0.9-x}Al_{1-x}Ti_{0.1+2x}$ and n-type $Fe_2V_{1.1-x}Al_{0.9-x}Ti_{2x}$ compositions.

For both sample series, we found significant enhancements of the thermoelectric figure of merit at lower levels of the two-fold (VAl)/Ti_2 substitution, compared to the non-substituted compounds ($x = 0$). Specifically, the temperature-dependent Seebeck coefficient ($S(T)$) showed notable improvements, with values reaching $S = 130$ μV/K in p-type samples, attributable to the induced band gap opening. This is particularly important for p-type samples, for which the low $S(T)$ previously inhibited high values of zT.

To further optimize the thermoelectric performance, heavy-element doping was explored through isovalent V/Ta substitution. A 5% substitution of V with Ta led to a substantial increase in zT up to $zT = 0.3$ in n-type and $zT = 0.18$ in p-type samples, which represent some of the highest reported values for both p- and n-type Fe_2VAl-based thermoelectrics.

CRediT authorship contribution statement

M. Parzer: Writing – review & editing, Writing – original draft, Visualization, Validation, Supervision, Software, Methodology, Investigation, Formal analysis, Data curation, Conceptualization. **A. Kositz:** Visualization, Validation, Investigation, Formal analysis, Data curation. **J. Süß:** Validation, Investigation, Formal analysis, Data curation. **F. Garmroudi:** Writing – review & editing, Methodology, Formal analysis, Conceptualization. **T. Mori:** Writing – review & editing, Project administration, Funding acquisition. **E. Bauer:** Writing – review & editing, Validation, Supervision, Project administration, Funding acquisition.

Declaration of competing interest

The authors declare that they have no known competing financial interests or personal relationships that could have appeared to influence the work reported in this paper.

Acknowledgments

This research was supported by the Japan Science and Technology Agency (JST) under the MIRAI program, Grant No. JPMJMI19A1. The authors thank Monika Waas and Robert Svagera for conducting the Scanning Electron Microscope (SEM) measurements.

Appendix A. Supplementary data

Supplementary material related to this article can be found online at https://doi.org/10.1016/j.mtphys.2025.101712.

Data availability

Data will be made available on request.

References

[1] B. Jiang, W. Wang, S. Liu, Y. Wang, C. Wang, Y. Chen, L. Xie, M. Huang, J. He, High figure-of-merit and power generation in high-entropy gete-based thermoelectrics, Sci. 377 (2022) 208.

[2] O. Meroz, N. Elkabets, Y. Gelbstein, Enhanced thermoelectric properties of n-type bi2te3–x se x alloys following melt-spinning, ACS Appl. Energy Mater. 3 (2019) 2090.

[3] H.-T. Liu, Q. Sun, Y. Zhong, Q. Deng, L. Gan, F.-L. Lv, X.-L. Shi, Z.-G. Chen, R. Ang, High-performance in n-type pbte-based thermoelectric materials achieved by synergistically dynamic doping and energy filtering, Nano Energy 91 (2022) 106706.

[4] D. Ben-Ayoun, Y. Sadia, Y. Gelbstein, Compatibility between co-metallized pbte thermoelectric legs and an ag–cu–in brazing alloy, Mater. 11 (2018) 99.

[5] M. Kaller, D. Fuks, Y. Gelbstein, Sc solubility in p-type half-heusler (ti1-cscc) nisn thermoelectric alloys, J. Alloys Compd. 729 (2017) 446.

[6] Y. Nishino, S. Kamizono, H. Miyazaki, K. Kimura, Effects of off-stoichiometry and Ti doping on thermoelectric performance of Fe_2VAl Heusler compound, AIP Adv. 9 (2019).

[7] B. Hinterleitner, I. Knapp, M. Poneder, Y. Shi, H. Müller, G. Eguchi, C. Eisenmenger-Sittner, M. Stöger-Pollach, Y. Kakefuda, N. Kawamoto, et al., Thermoelectric performance of a metastable thin-film heusler alloy, Nat. 576 (2019) 85.

[8] M. Parzer, F. Garmroudi, A. Riss, S. Khmelevskyi, T. Mori, E. Bauer, High solubility of al and enhanced thermoelectric performance due to resonant states in fe2valx, Appl. Phys. Lett. 120 (2022).

[9] A. Diack-Rasselio, O. Rouleau, L. Coulomb, L. Georgeton, M. Beaudhuin, J.-C. Crivello, E. Alleno, Influence of self-substitution on the thermoelectric Fe_2VAl Heusler alloy, J. Alloys Compd. 920 (2022) 166037.

[10] K. Fukuta, K. Tsuchiya, H. Miyazaki, Y. Nishino, Improving thermoelectric performance of fe2val-based heusler compounds via high-pressure torsion, Appl. Phys. A 128 (2022) 1.

[11] F. Garmroudi, M. Parzer, A. Riss, S. Beyer, S. Khmelevskyi, T. Mori, M. Reticcioli, E. Bauer, Large thermoelectric power factors by opening the band gap in semimetallic heusler alloys, Mater. Today Phys. 27 (2022) 100742.

[12] E. Alleno, A. Diack-Rasselio, M.T. Noutack, P. Jund, Optimization of the thermoelectric properties in self-substituted Fe_2VAl, Phys. Rev. Mater. 7 (2023) 075403.

[13] D. Bourgault, H. Hajoum, R. Haettel, E. Alleno, Unlocking microwatt power: enhanced performance of Fe–V–Al thin films in thermoelectric microgenerators, J. Mater. Chem. A 11 (2023) 19556.

[14] F. Garmroudi, A. Riss, M. Parzer, N. Reumann, H. Müller, E. Bauer, S. Khmelevskyi, R. Podloucky, T. Mori, K. Tobita, et al., Boosting the thermoelectric performance of Fe_2VAl-type heusler compounds by band engineering, Phys. Rev. B 103 (2021) 085202.

[15] M. Parzer, Extending the Phase Space of Thermoelectric Full-Heusler Compounds (Ph.D. thesis), Technische Universität Wien, 2024.

[16] A. Jain, S.P. Ong, G. Hautier, W. Chen, W.D. Richards, S. Dacek, S. Cholia, D. Gunter, D. Skinner, G. Ceder, et al., Commentary: The materials project: A materials genome approach to accelerating materials innovation, APL Mater. 1 (2013).

[17] J.L. Murray, The fe- ti (iron-titanium) system, Bull. Alloy. Phase Diagr. 2 (1981) 320.

[18] C. Chien, S. Liou, Crystalline and amorphous feti and fe 2 ti, Phys. Rev. B 31 (1985) 8238.

[19] J. Liebertz, S. Stähr, S. Haussühl, Growth and properties of single crystals of feti, Krist. Tech. 15 (1980) 1257.

[20] I. Galanakis, P. Dederichs, N. Papanikolaou, Slater-pauling behavior and origin of the half-metallicity of the full-heusler alloys, Phys. Rev. B 66 (2002) 174429.

[21] T. Graf, C. Felser, S.S. Parkin, Simple rules for the understanding of heusler compounds, Prog. Solid State Chem. 39 (2011) 1.

[22] M. Weinert, R. Watson, Hybridization-induced band gaps in transition-metal aluminides, Phys. Rev. B 58 (1998) 9732.

[23] M. Parzer, F. Garmroudi, A. Riss, M. Reticcioli, R. Podloucky, M. Stöger-Pollach, E. Constable, A. Pustogow, T. Mori, E. Bauer, Semiconducting heusler compounds beyond the slater-pauling rule, PRX Energy 3 (2024) 033006.

[24] H. Matsuura, Doping effects on thermoelectric properties of the pseudogap fe2val system, J. Jpn. Inst. Met. 66 (2002) 767.

[25] H. Miyazaki, S. Tanaka, N. Ide, K. Soda, Y. Nishino, Thermoelectric properties of heusler-type off-stoichiometric fe2v1+ xal1- x alloys, Mater. Res. Express 1 (2013) 015901.

[26] M. Mikami, M. Inukai, H. Miyazaki, Y. Nishino, Effect of off-stoichiometry on the thermoelectric properties of heusler-type fe 2 val sintered alloys, J. Electron. Mater. 45 (2016) 1284.

[27] B. Hinterleitner, P. Fuchs, J. Rehak, F. Garmroudi, M. Parzer, M. Waas, R. Svagera, S. Steiner, M. Kishimoto, R. Moser, et al., Stoichiometric and off-stoichiometric full Heusler $Fe_2V_{1-x}W_xAl$ thermoelectric systems, Phys. Rev. B 102 (2020) 075117.

[28] V. Niculescu, T. Burch, K. Raj, J. Budnick, Properties of heusler-type materials fe2tsi and feco2si, J. Magn. Magn. Mater. 5 (1977) 60.

[29] M. Meinert, M.P. Geisler, J. Schmalhorst, U. Heinzmann, E. Arenholz, W. Hetaba, M. Stöger-Pollach, A. Hütten, G. Reiss, Experimental realization of a semiconducting full-Heusler compound: Fe_2TiSi, Phys. Rev. B 90 (2014) 085127.

[30] L. Vegard, Die konstitution der mischkristalle und die raumfüllung der atome, Z. Phys. 5 (1921) 17.

[31] See supplemental material at [URL will be inserted by publisher] for additional results regarding thermoelectric properties of the samples with higher (VAl)/Ti substitution and for the detailed thermoelectric properties of the Ta substituted samples (including references *citations*).

[32] M. Parzer, A. Riss, F. Garmroudi, J. de Boor, T. Mori, E. Bauer, Seeband: A highly efficient, interactive tool for analyzing electronic transport data, 2024, https://arxiv.org/abs/2409.06261.

[33] A.F. May, G.J. Snyder, Introduction to modeling thermoelectric transport at high temperatures, in: D.M. Rowe (Ed.), Materials, Preparation, and Characterization in Thermoelectrics, CRC Press, 2012, Chap. 11.

[34] Y. Takagiwa, Y. Iwasaki, Effect of Off-Stoichiometry and Point Defects on Thermoelectric Properties of a W-Substituted Fe_2VAl Heusler Compound, ACS Appl. Energy Mater. 6 (2023) 8256.

[35] J. Callaway, H.C. von Baeyer, Effect of point imperfections on lattice thermal conductivity, Phys. Rev. 120 (1960) 1149.

[36] P. Klemens, Thermal resistance due to point defects at high temperatures, Phys. Rev. 119 (1960) 507.

[37] F. Garmroudi, M. Parzer, A. Riss, N. Reumann, B. Hinterleitner, K. Tobita, Y. Katsura, K. Kimura, T. Mori, E. Bauer, Solubility limit and annealing effects on the microstructure & thermoelectric properties of $Fe_2V_{1-x}Ta_xAl_{1-y}Si_y$ heusler compounds, Acta Mater. 212 (2021) 116867.

[38] Y. Terazawa, M. Mikami, T. Itoh, T. Takeuchi, Effects of heavy element substitution on electronic structure and lattice thermal conductivity of fe 2 val thermoelectric material, J. Electron. Mater. 41 (2012) 1348.

[39] K. Kimura, K. Yamamoto, K. Hayashi, S. Tsutsui, N. Happo, S. Yamazoe, H. Miyazaki, S. Nakagami, J. Stellhorn, S. Hosokawa, et al., Local structure and atomic dynamics in fe 2 val heusler-type thermoelectric material: The effect of heavy element doping, Phys. Rev. B 101 (2020) 024302.